Chem. Mater. **1994,** *6,* 2222−2226

Electrocrystallization of an Ordered Organic Monolayer: Selective Epitaxial Growth of β-$(ET)_2I_3$ on Graphite

Andrew C. Hillier, Jeffery B. Maxson, and
Michael D. Ward*

Department of Chemical Engineering and
Materials Science, University of Minnesota
Amundson Hall, 421 Washington Ave. SE
Minneapolis, Minnesota 55455

Received August 10, 1994
Revised Manuscript Received October 4, 1994

The fabrication of highly ordered organic thin films has received considerable attention in attempts to develop materials for molecular-based electronic devices, sensors, displays, and logic elements.[1] Examples of two-dimensional films with potentially desirable electronic properties include self-assembled mono- and multilayers with redox-active components[2] and thin films of organic dyes grown by molecular beam epitaxy on van der Waals substrates such as graphite, MoS_2, and SnS_2.[3] Successful approaches to the manufacturing of devices based on organic thin films will ultimately rely on the development of convenient fabrication methods as well as rigorous control of the supramolecular structure of the thin-film assembly. The importance of supramolecular structure is evident from the behavior of crystalline low-dimensional organic conductors, whose electronic properties, such as conductivity and superconductivity, differ considerably among polymorphs of a given composition.[4] This is exemplified by charge-transfer salts of the ET−I_3 system (ET = bis(ethylenedithiolo)tetrathiafulvalene), for which 14 phases are known, four exhibiting superconductivity.[5] Indeed, the synthesis of these materials by electrochemical oxidation of ET in the presence of I_3^- is characterized by the simultaneous growth of single crystals of several different polymorphs at the electrode surface.[4a,6]

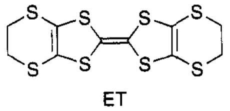

ET

Recent observations in our laboratory indicated that the vapor-phase growth of certain low-dimensional organic crystals on highly ordered substrates was preceded by the formation of mono- and multilayer films with rather large dimensions.[7] This, along with a report describing the influence of electrode composition on phase selectivity during the growth of $(ET)_2I_3$,[8] prompted us to examine whether polymorphism in this compound could be controlled at the early stages of growth by favorable interactions with the substrate electrode. We report herein electrochemical and in situ atomic force microscopy observations of the electrocrystallization of a novel crystalline organic monolayer comprising $(ET)_2I_3$ on highly oriented pyrolytic graphite (HOPG) electrodes, in which epitaxy between $(ET)_2I_3$ and the HOPG substrate directs selectivity toward a single polymorph. These results suggest a new strategy for the convenient preparation of highly ordered organic films with adjustable electronic properties.

The electrocrystallization of $(ET)_2I_3$ occurs with the simultaneous formation of several phases, with α and β phases predominating. Previous reports have indicated that the α-phase forms preferentially at large overpotentials ($E_{app} \gg E_{0,ET/ET^+}$) and in the presence of chemical oxidants, including I_2.[4a,9] Conversely, β-$(ET)_2I_3$ is favored at low overpotentials. This selectivity suggests that α-$(ET)_2I_3$ is kinetically favored, while β-$(ET)_2I_3$ is thermodynamically preferred and, therefore, grows under conditions closer to equilibrium.[10] Notably, electrocrystallization of $(ET)_2I_3$ at graphite electrodes has been shown to favor the formation of β-$(ET)_2I_3$, whereas electrochemically oxidized graphite electrodes afforded α-$(ET)_2I_3$.[8] This behavior suggests that interfacial interactions between β-$(ET)_2I_3$ and graphite during heterogeneous nucleation may be a significant factor in determining selectivity.

In acetonitrile, ET exhibits two reversible oxidations (eqs 1 and 2), whereas I_3^- exhibits a single reversible oxidation to I_2 (eq 3.) The oxidation of both ET and I_3^-

$$\mathrm{ET} \rightarrow \mathrm{ET}^+ + e^- \qquad E_0 = 650\ \mathrm{mV\ (vs\ Ag/AgCl)} \tag{1}$$

$$\mathrm{ET}^+ \rightarrow \mathrm{ET}^{2+} + e^- \qquad E_0 = 890\ \mathrm{mV} \tag{2}$$

$$2I_3^- \rightarrow 3I_2 + 2e^- \qquad E_0 = 860\ \mathrm{mV} \tag{3}$$

$$2(\mathrm{ET}) + I_3^- \rightarrow (\mathrm{ET})_2I_3 + e^- \qquad E_{cryst} \approx 650\ \mathrm{mV} \tag{4}$$

at a freshly cleaved HOPG electrode (Figure 1A,B) occurs at potentials similar to those observed at polycrystalline electrodes, with slight electrochemical ir-

---

* To whom correspondence should be addressed.

(1) (a) Aviram, A.; Ratner, M. A. *Chem. Phys. Lett.* **1974**, *29*, 277. (b) Carter, F. L., Ed. *Molecular Electronic Devices*; Marcel Dekker: New York, 1982. (c) Ashwell, G. J., Ed. *Molecular Electronics*; John Wiley & Sons: New York, 1992.

(2) (a) Matsumoto, M.; Nakamura, T.; Manda, E.; Kawabata, Y. *Thin Solid Films* **1988**, *160*, 61. (b) Naito, K.; Miura, A.; Azuma, M. *J. Am. Chem. Soc.* **1991**, *113*, 6386. (c) Dhindsa, A. S.; Song, Y.-P.; Badyal, J. P.; Bryce, M. R.; Lvov, Y. M.; Petty, M. C.; Yarwood, J. *Chem. Mater.* **1992**, *4*, 724. (d) Yip, C. M.; Ward, M. D. *Langmuir* **1994**, *10*, 549.

(3) (a) Collins, G. E.; Nebesny, J. W.; England, C. D.; Chau, L. K.; Lee, P. A.; Parkinson, B. A.; Armstrong, N. R. *J. Vac. Sci. Technol. A* **1992**, *10*, 2902. (b) Ludwig, C.; Gompf, B.; Glatz, W.; Petersen, J.; Eisenmenger, W.; Mobus, M.; Zimmerman, U.; Karl, N. *Z. Phys. B* **1992**, *86*, 397. (c) Ludwig, C.; Gompf, B.; Petersen, J.; Strohmaier, R.; Eisenmenger, W. *Z. Phys. B.* **1994**, *93*, 365. (d) Armstrong, N. R.; Nebesny, K. W.; Collins, G. E.; Chau, L.-K.; Lee, P. A.; England, C.; Diehl, D.; Douskey, M.; Parkinson, B. A. *Thin Solid Films* **1992**, *216*, 90. (e) Nebesny, K. W.; Collins, G. E.; Lee, P. A.; Chau, L.-K.; Danziger, J.; Osburn, E.; Armstrong, N. R. *Chem. Mater.* **1991**, *3*, 829.

(4) (a) Williams, J. M.; Wang, H. H.; Emge, T. J.; Geiser, U.; Beno, M. A.; Leung, C. W.; Carlson, K. D.; Thorn, R. J.; Schultz, A. J. In *Progress in Inorganic Chemistry*; Lippard, S. J., Ed.; John Wiley and Sons: New York, 1987; p 51. (b) Williams, J. M.; Schultz, A. J.; Geiser, U.; Carlson, K. D.; Kini, A. M.; Wang, H. H.; Kwok, W.-K.; Whangbo, M.-H.; Schirber, J. E. *Science* **1991**, *252*, 1501.

(5) (a) Carlson, K. D.; Wang, H. H.; Beno, M. A.; Kini, A. M.; Williams, J. M. *Mol. Cryst. Liq. Cryst.* **1990**, *181*, 91. (b) Shibaeva, R. P.; Yagubskii, E. B.; Laukhina, E. E.; Laukhin, V. N. In *The Physics and Chemistry of Organic Superconductors*; Saito, G., Kagoshima, S., Eds.; Springer-Verlag: Berlin, 1990; p 342.

(6) (a) Williams, J. M.; Emge, T. J.; Wang, H. H.; Beno, M. A., Coops, P. T.; Hall, L. N.; Carlson, K. D.; Crabtree, G. W. *Inorg. Chem.* **1984**, *23*, 2560. (b) Shibaeva, R. P.; Kaminskii, V. F.; Bel'skii, V. K. *Sov. Phys. Crystallogr.* **1984**, *29*, 638. (c) Kobayashi, A.; Kato, R.; Kobayashi, H.; Moriyama, S.; Nishio, Y.; Kajita, K.; Sasaki, W. *Chem. Lett.* **1986**, 2017. (d) Kobayashi, A.; Kato, R.; Kobayashi, H.; Moriyama, S.; Nishio, Y.; Kajita, K.; Sasaki, W. *Ibid.* **1987**, 459.

(7) (a) Hossick-Schott, J.; Ward, M. D. *J. Am. Chem. Soc.* **1994**, *116*, 6806. (b) Hossick-Schott, J.; Ward, M. D. *Langmuir*, in press.

(8) Wang, H. H.; Montgomery, L. K.; Husting, C. A.; Vogt, B. A.; Williams, J. M.; Budz, S. M.; Lowry, M. J.; Carlson, K. D.; Kwok, W.-K.; Mikheyev, V. *Chem. Mater.* **1989**, *1*, 484.

0897-4756/94/2806-2222$04.50/0

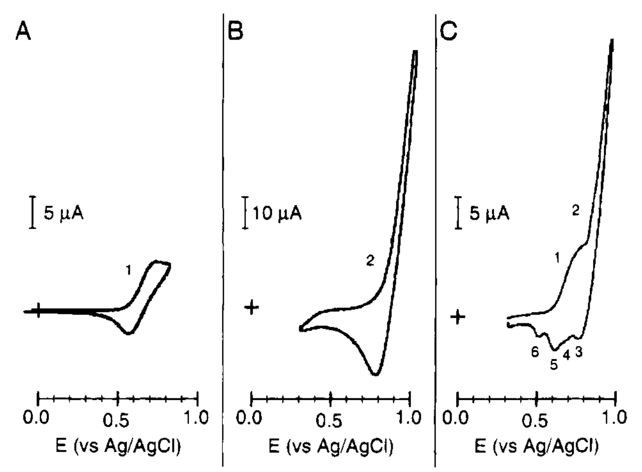

Figure 1. Cyclic voltammetry of ET and n-$Bu_4N^+I_3^-$ in CH_3CN at a 9 mm diameter freshly cleaved HOPG electrode: (A) 0.5 mM ET in 0.1 M n-$Bu_4N^+ClO_4^-$; (B) 10 mM n-$Bu_4N^+I_3^-$ in 0.1 M n-$Bu_4N^+ClO_4^-$; (C) 0.5 mM ET and 10 mM n-$Bu_4N^+I_3^-$ in 0.1 M n-$Bu_4N^+ClO_4^-$. The electrochemical cell consisted of a single compartment with a freshly cleaved HOPG working electrode and a platinum counter electrode. The potential scale is against the reference electrode, which was Ag/AgCl in 0.1 M n-$Bu_4N^+Cl^-/CH_3CN$.

reversibility. This irreversibility is typical of redox processes occuring at highly crystalline graphite and is attributed to slow kinetics at the exposed basal plane.[11] Cyclic voltammetry performed in acetonitrile containing both ET and I_3^- (Figure 1C) indicates the oxidation of ET (peak 1) and I_3^- (peak 2). Crystallization of $(ET)_2I_3$ occurs following the oxidation of ET (eq 4). Consequently, $(ET)_2I_3$ forms at the foot of the I_3^- oxidation wave, where the concentration of I_2 at the electrode surface is not substantial, although I_2-mediated oxidation of ET cannot be explicitly ruled out.[9]

Reversing the scan direction following excursions into the I_3^-/I_2 couple results in four reduction peaks. The first peak (peak 3), corresponds to the reduction of I_2 (eq 5). This is followed by a shoulder and a peak at

$$3I_2 + 2e^- \rightarrow 2I_3^- \qquad E' = 800\text{ mV} \qquad (5)$$

$$ET^+ + e^- \rightarrow ET \qquad E' = 670\text{ mV} \qquad (6)$$

$$(ET)_2I_3 + e^- \rightarrow 2(ET) + I_3^- \qquad E' = 620\text{ mV} \qquad (7)$$

$$(ET)_2I_3(\text{monolayer}) + e^- \rightarrow 2(ET) + I_3^- \qquad E' = 500\text{ mV} \qquad (8)$$

slightly more cathodic potentials, corresponding to the reduction of free ET^+ remaining in the depletion layer near the electrode surface (peak 4, eq 6) and reduction of bulk $(ET)_2I_3$ on the electrode surface (peak 5, eq 7). The assignment of peak 5 was corroborated by the observation that scanning the potential at a faster rate, which decreased the time available for crystallization, resulted in a decrease in the magnitude of peak 5 and a corresponding increase in peak 4. A fourth and final reduction peak (peak 6) is attributed to the reduction and dissolution of a $(ET)_2I_3$ monolayer (eq 8) on the graphite surface. Integration of the current under peak 6 gives a coverage of $\Gamma = 4.39 \times 10^{-10}$ mol cm^{-2} for $(ET)_2I_3$.

In situ atomic force microscopy (AFM) of a freshly cleaved HOPG electrode confirms that a monolayer of $(ET)_2I_3$ forms upon the application of an anodic potential (Figure 2).[12] Imaging of the substrate prior to electrodeposition reveals an atomically smooth surface over the length scale under examination (2.5 μm), with a single 7 Å step oriented along one of the graphite lattice vectors corresponding to the $\{\bar{1}2\bar{1}0\}$ family of directions. Following the application of an anodic potential step of $E_{app} \approx 650$ mV (vs Ag/AgCl), clusters exhibiting a 15.5 Å height form at discrete locations on the surface (Figure 2E). These clusters nucleate directly upon substrate terrace sites and grow laterally along the surface with their facet directions exhibiting an azimuthal orientation of $\approx 10° \pm n60°$ with respect to the graphite lattice (Figure 2C). Eventually the entire HOPG surface becomes covered, with grain boundaries appearing between individual clusters and at substrate step sites. These grain boundaries anneal with time to provide a monolayer that appears to be defect free by AFM observation and is stable indefinitely at $E > 650$ mV. The monolayer can be formed and removed repeatedly upon potential cycling.

High resolution AFM imaging of the $(ET)_2I_3$ monolayer (Figure 3A) reveals a structure resembling that observed for the (001) face of single-crystal β-$(ET)_2I_3$. The most prominent contrast in the direct space AFM data exhibits a periodicity having lattice parameters of $\mathbf{b_1} = 12.0\ (\pm 0.8)$ Å, $\mathbf{b_2} = 8.5\ (\pm 0.8)$ Å, and $\gamma = 108°\ (\pm 3)$. This lattice corresponds to the smallest reciprocal cell observed in the Fourier analysis of the data. These parameters compare favorably to the single-crystal X-ray parameters of the β-$(ET)_2I_3$ (001) face of $a = 6.6$ Å ($\cong {}^1/_2\mathbf{b_1}$), $b = 9.1$ Å ($\cong \mathbf{b_2}$), and $\gamma = 110°$ (Figure 4A). Although $\mathbf{b_1}$ is twice the expected crystallographic $\mathbf{a}$ value, Fourier analysis also reveals a larger reciprocal cell corresponding to a unit cell in real space with $\mathbf{b_3} = 6.0\ (\pm 0.4)$ Å, $\mathbf{b_2} = 8.5\ (\pm 0.8)$ Å, and $\gamma = 108°\ (\pm 3)$, in near exact agreement with the crystallographic parameters of the (001) face of β-$(ET)_2I_3$. The direct and Fourier space data also reflect the $p1$ plane symmetry of the (001) plane of β-$(ET)_2I_3$, in contrast to the nearly $p2$ plane symmetry ($\gamma = 90.85°$) expected for the (001) layer of α-$(ET)_2I_3$.[13] The ordered nature of the monolayer is evident from the symmetry of the higher order components in the Fourier data. The assignment of the

---

(9) (a) Endres, H.; Hiller, M.; Keller, H. J.; Bender, K.; Gogu, E.; Heinen, I.; Schweitzer *Z. Naturforsch.* **1985**, *40b*, 1664. (b) Shibaeva, R. P.; Kaminskii, V. F.; Yagubskii, E. B. *Mol. Cryst. Liq. Cryst.* **1985**, *119*, 361.

(10) Wang, H. H.; Ferraro, J. R.; Carlson, K. D.; Montgomery, L. K.; Geiser, U.; Williams, J. M.; Whitworth, J. R.; Schlueter, J. A.; Hill, S.; Whangbo, M.-H.; Evain, M.; Novoa, J. J. *Inorg. Chem.* **1989**, *28*, 2267.

(11) McCreery, R. L. In *Electroanalytical Chemistry: A Series of Advances*; Bard, A. J., Ed.; Marcel Dekker: New York, 1991; Vol. 17, p 303.

(12) AFM experiments were performed with a Digital Instruments Nanoscope III scanning probe microscope equipped with Nanoprobe cantilevers (Si_3N_4 integral tips with spring constants of 0.06 nm^{-1}, PARK Scientific). Images were obtained at high feedback, such that the tip tracked the sample at constant force. A scanner with maximum scanning range of 12 × 12 × 4.4 μm^3 was employed for imaging. The tip scan rate during image acquisition ranged from 4 to 12 Hz for large scale images and up to 40 Hz for high-resolution images, while the applied tip–sample force was maintained at $F_{tip} \leq 5$ nN in solution. AFM experiments were performed in acetonitrile with a fluid cell (Digital Instruments), comprising a quartz body with ports for fluid entry and exit. The working electrode consisted of a freshly cleaved HOPG wafer. Platinum counter and Ag reference electrodes were inserted through the outlet port of the fluid cell.

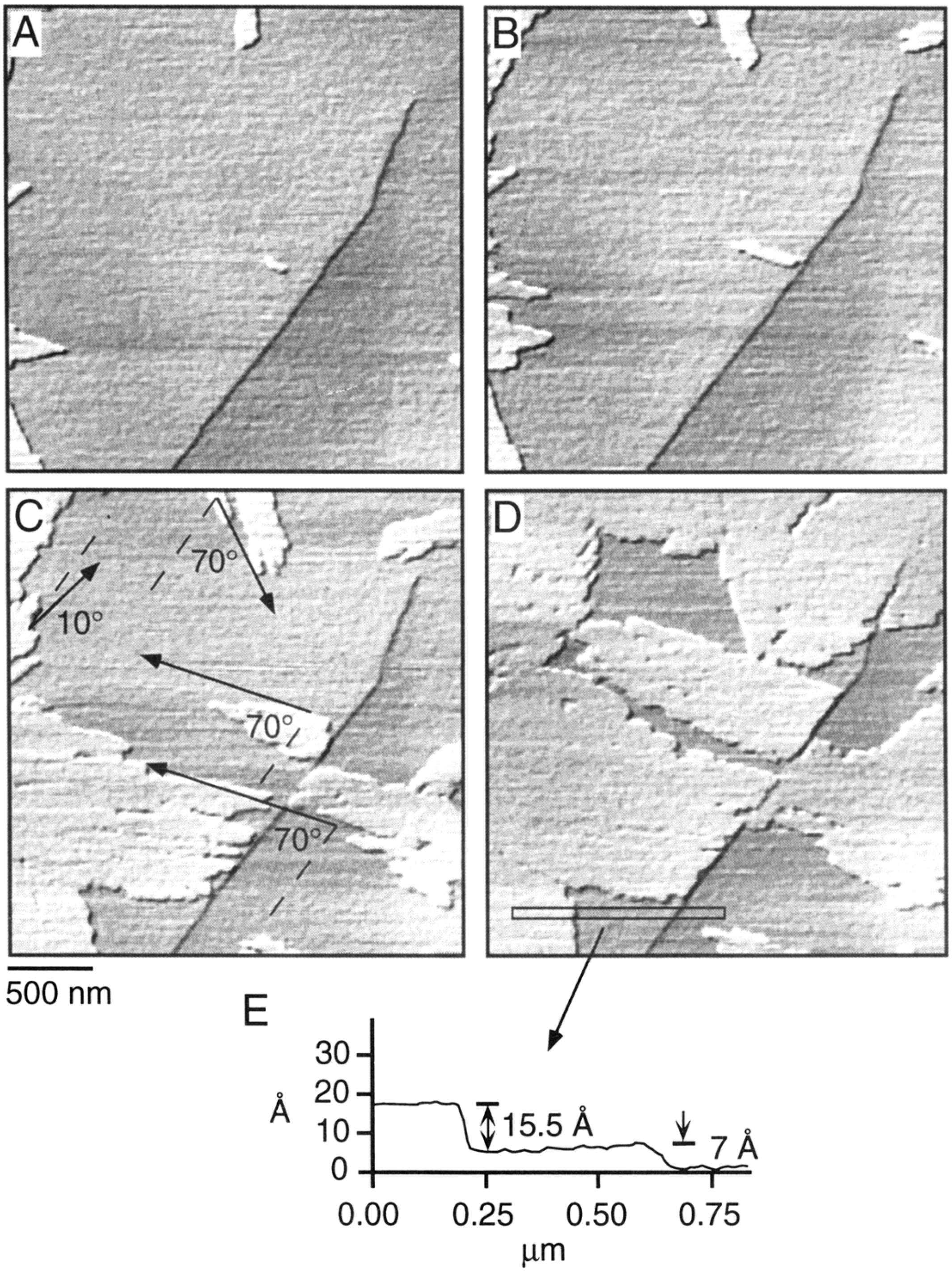

Figure 2. In situ AFM images acquired during growth of the $(ET)_2I_3$ monolayer on a freshly cleaved HOPG electrode at (A) t = 30, (B) 90, (C) 150, and (D) 210 s following a potential step to 650 mV (vs Ag/AgCl). Note that (A) does not represent the actual beginning of monolayer formation, but the time at which the first image was acquired shortly after the potential step. In (C), the angles between the orientation of a primary HOPG lattice vector (- - -) and the directions of monolayer faceting (— —) are indicated. (E) Height profile analysis of the $(ET)_2I_3$ monolayer and a neighboring graphite step from (D).

monolayer to a β-like structure is further corroborated by the 15.5 Å monolayer height (Figure 2E), which is identical to the (001) layer height of 15.3 Å for β-$(ET)_2I_3$ (Figure 4B). The monolayer coverage determined from this high resolution image is $\Gamma = 3.3 \times 10^{-10}$ mol cm^{-2}, which is similar to that deduced from voltammetry (vide supra) and from the molecular density of the (001) plane of β-$(ET)_2I_3$, which gives $\Gamma = 3.00 \times 10^{-10}$ mol cm^{-2}.

At applied potentials exceeding 650 mV and after the $(ET)_2I_3$ monolayer is completely formed, microscopic single crystals emerge at discrete locations on the HOPG substrate. At moderate to low overpotentials, growth of these crystals occurs by a layering mechanism wherein 15.5 Å thick β-$(ET)_2I_3$ (001) layers emerge from a single screw dislocation and spread across the crystal surface. These microcrystals were identified as β-$(ET)_2I_3$, based upon AFM goniometry[14] and from high-resolution imaging of the exposed (001) face of these crystals.

---

(13) Crystallographic parameters for α-$(ET)_2I_3$: a = 9.183 Å, b = 10.804 Å, c = 17.442 Å; α = 96.96°, β = 97.93°, γ = 90.85°. Emge, T. J.; Heung, P. C. W.; Beno, M. A.; Wang, H. H.; Williams, J. M.; Whangbo, M.-H.; Evain, M. *Mol. Cryst. Liq. Cryst.* **1986**, *138*, 393.

(14) Hillier, A. C.; Ward, M. D. *Science* **1994**, *263*, 1261.

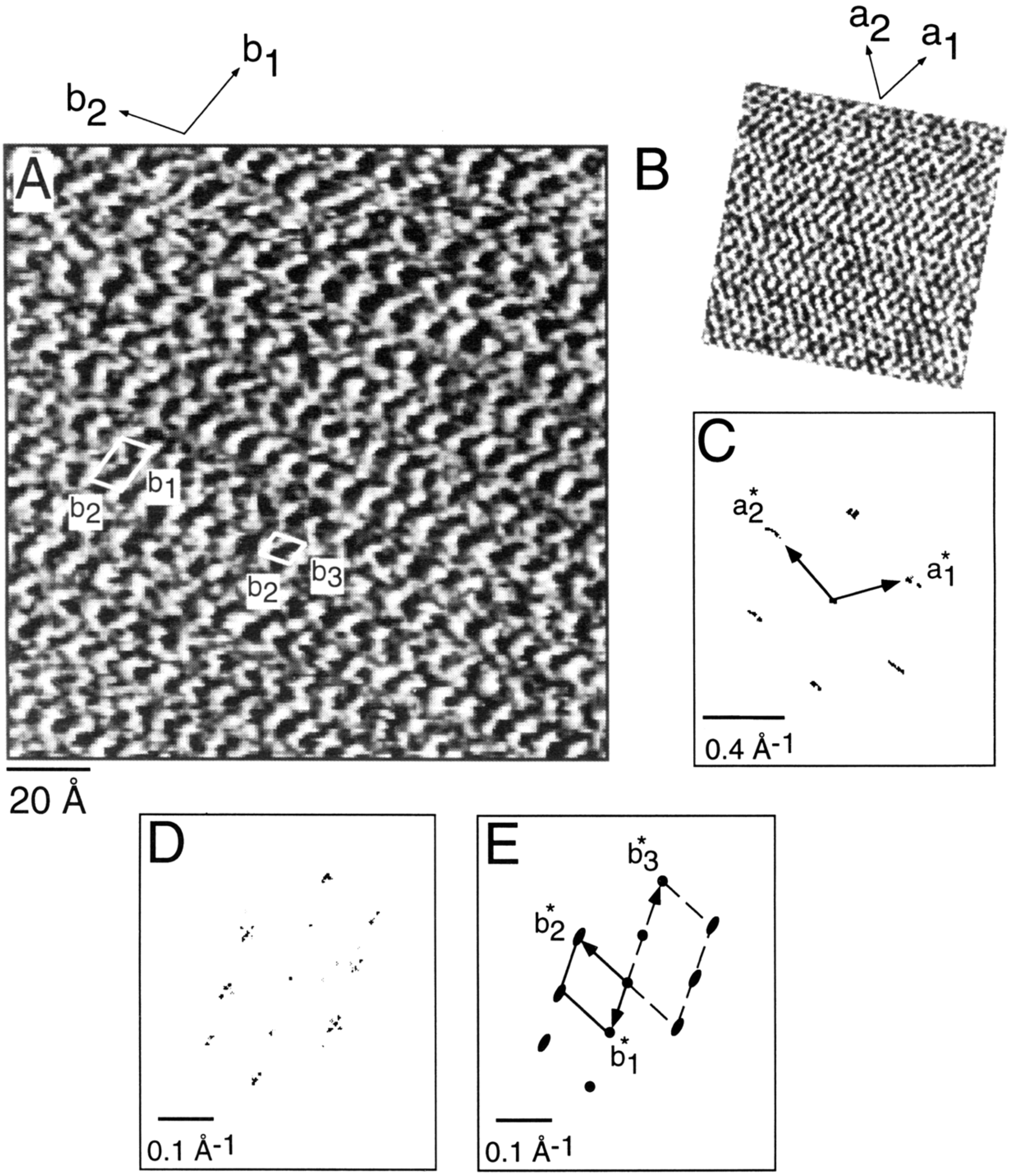

Figure 3. (A) In situ high-resolution AFM data (raw data) for the β-(ET)$_2$I$_3$ monolayer. The data exhibit a contrast periodicity of $\mathbf{b_1}$ = 12.0 (±0.8) Å and $\mathbf{b_2}$ = 8.5 Å (±0.8) with γ = 108° (±3). The variation in contrast corresponds to changes is surface topography, with brighter regions being closer to the AFM tip. Two unit cells are depicted: the larger one corresponding to the smallest reciprocal cell determined from Fourier analysis and the smaller one corresponding to a reciprocal cell having dimensions identical to those of the (001) plane of β-(ET)$_2$I$_3$ (see Figure 4A). This cell compares favorably with the (001) plane, for which a = 6.6 Å ($\approx\mathbf{b_3} = {}^1\!/_2\mathbf{b_1}$), b = 9.1 Å ($\approx\mathbf{b_2}$), and γ = 110°. (B) AFM data (raw data) and (C) Fourier analysis obtained for the HOPG substrate after removal of the monolayer by mechanical etching with the AFM tip. The reciprocal lattice directions, $\mathbf{a_1}^*$ and $\mathbf{a_2}^*$, are indicated on the Fourier data, while the real lattice directions, $\mathbf{a_1}$ and $\mathbf{a_2}$, are shown above the real space image. The HOPG image is rotated to match the scan direction employed while imaging the monolayer in (A). (D) Fourier data for the (ET)$_2$I$_3$ monolayer. (E) Schematic of the Fourier data of (D) depicting the reciprocal lattices corresponding to the two cells indicated in the real space image. The reciprocal lattice vectors $\mathbf{b_1}^*$, $\mathbf{b_2}^*$, $\mathbf{b_3}^*$, corresponding to the real lattice vectors in (A), are depicted. The larger reciprocal cell corresponds to the real cell having the dimensions of the (001) plane of β-(ET)$_2$I$_3$. On the basis of the real and reciprocal lattice vectors, the (ET)$_2$I$_3$ monolayer exhibits an average azimuthal orientation, with respect to the HOPG substrate, of $\mathbf{b_1} = 4.9\mathbf{a_1} + 1.1\mathbf{a_2}$ and $\mathbf{b_2} = 3.86(\mathbf{a_2} - \mathbf{a_1})$. The angular spread about this average orientation was ±10°.

Notably, the AFM contrast and Fourier analysis of high-resolution images of these crystals were identical to that observed for the monolayer. This growth mechanism resembles the classical Stranski–Krastanov growth mechanism,[15] in which bulk crystallization is preceded by the formation of a single monolayer as a consequence of strong interaction between the substrate and the first

---

(15) Lewis, B.; Anderson, J. C. *Nucleation and Growth of Thin Films*; Academic Press: New York, 1978.

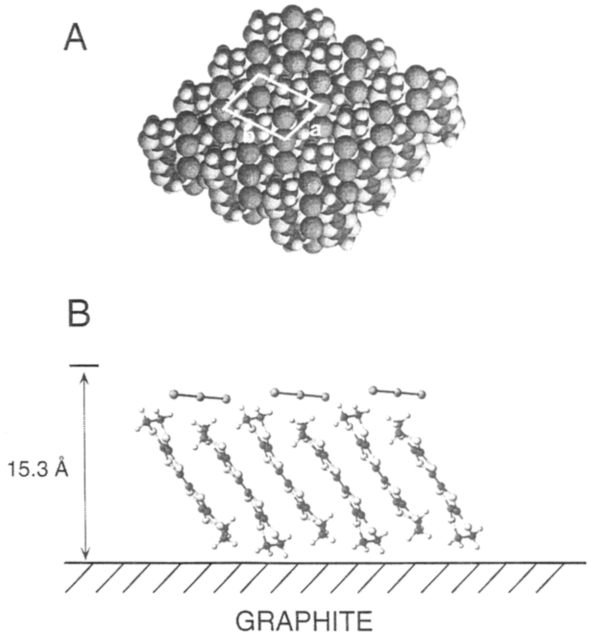

Figure 4. (A) Space-filling representation of the (001) face of β-$(ET)_2I_3$ terminated with I_3^- anions. The unit cell with the lattice parameters given in the caption of Figure 3 is depicted. The lattice constants of the cell agree with those observed in the AFM data of the β-$(ET)_2I_3$ monolayer in Figure 3A, with $\mathbf{2a} = \mathbf{b}_1$ and $\mathbf{b} = \mathbf{b}_2$. (B) Schematic representation of a (001) layer of β-$(ET)_2I_3$ from the single-crystal X-ray structure, on the HOPG substrate. The monolayer height measured by AFM (15.5 Å) is identical to the thickness of this (001) layer in the bulk crystal (15.3 Å). The ET molecules are positioned with their long axis nearly parallel to the HOPG substrate and are separated from the next layer by a sheet of I_3^- anions. The monolayer is depicted here with I_3^- anions at the upper surface, although this assignment is not yet definitive.

crystal layer. Full details of the crystal growth of β-$(ET)_2I_3$ on HOPG will be presented in a later publication.[16]

The observed growth mode and the preferred monolayer facetting of 10° ± n60° with respect to the graphite lattice vectors suggest that the formation of the β-$(ET)_2I_3$ monolayer is driven by epitaxy with the HOPG substrate. To determine the azimuthal relationship between the HOPG and monolayer lattices, the AFM tip was rastered over a small region of the monolayer at a higher force (F > 20 nN) than that used for imaging. This resulted in mechanical removal of the monolayer and allowed high-resolution imaging of the HOPG substrate directly beneath the monolayer (Figure 3B). High-resolution AFM data of the monolayer and HOPG, along with analysis of the Fourier images, reveals an average azimuthal orientation of the monolayer with respect to the HOPG substrate described by $\mathbf{b}_1 = 4.9\mathbf{a}_1 + 1.1\mathbf{a}_2$, and $\mathbf{b}_2 = 3.86\ (\mathbf{a}_2 - \mathbf{a}_1)$, where $\mathbf{a}_1$ and $\mathbf{a}_2$ are the graphite lattice vectors of the basal plane ($|\mathbf{a}_1| = |\mathbf{a}_2| = 2.45$ Å), which are the $[\bar{1}2\bar{1}0]$ and $[2\bar{1}\bar{1}0]$ directions. The angular spread about this average orientation was ±10°. This alignment agrees with the orientations of the monolayer with respect to the graphite step directions, which are directed along $\mathbf{a}_1$, $\mathbf{a}_2$, and $\mathbf{a}_2 - \mathbf{a}_1$ (Figure 2C). Furthermore, microscopic crystals of β-$(ET)_2I_3$ that evolve from the monolayer are oriented with their (001) faces parallel to the graphite substrate and exhibit the same azimuthal orientation with respect to the graphite substrate. A geometric analysis of the β-$(ET)_2I_3$-graphite interface based on X-ray crystallographic data indicated that commensurism is maximized for an azimuthal orientation in which $\mathbf{2a}\ (=\mathbf{b}_1) = \mathbf{5a}_1 + \mathbf{a}_2$ and $\mathbf{b}\ (=\mathbf{b}_2) = {}^{11}/_{3}(\mathbf{a}_2 - \mathbf{a}_1)$. This transforms to a supercell with dimensions of $\mathbf{b}_1 \times \mathbf{3b}_2$ (Figure 3). A similar analysis did not reveal any reasonable commensurism of α-$(ET)_2I_3$ with the graphite lattice, consistent with the absence of α-$(ET)_2I_3$ during electrocrystallization on graphite.[8]

We note that occasionally a thin (<3 Å) layer is observed on HOPG at open circuit, which precedes formation of the β-$(ET)_2I_3$ monolayer. While in a few instances the 15.5 Å β-$(ET)_2I_3$ monolayer appears to form on top of this thin layer, most data indicate that this layer is either transformed into or displaced by the 15.5 Å monolayer.[17] For example, a 15.5 Å height with respect to the graphite surface was measured for the monolayer in Figure 3 after mechanical etching of a small region. The identity of this intermediate layer and its role in the formation of the β-$(ET)_2I_3$ monolayer is under examination.

These observations clearly indicate that an epitaxial interaction between β-$(ET)_2I_3$ and the basal plane of HOPG is responsible for the observed selectivity on pristine graphite substrates. This interaction results in the formation of a monolayer covering large areas of the substrate and exhibiting structural characteristics that mimic β-$(ET)_2I_3$, which in its bulk form is a superconductor at low temperature. The ability to prepare large highly ordered organic mono- and multilayers whose structure mimics that of an organic solid that has been demonstrated to exhibit metallic conductivity and superconductivity has interesting implications for the fabrication of electronic devices based on molecular components. Furthermore, the ability to employ electrochemical means has the advantage over typical vacuum deposition techniques in that deposition can be performed under ambient conditions and on substrates with unusual geometries.

Acknowledgment. The authors gratefully acknowledge the support of the Office of Naval Research and the Center for Interfacial Engineering (NSF Engineering Research Centers Program).

---

(16) Hillier, A. C.; Maxson, J. B.; Ward, M. D., to be submitted.

(17) The 3 Å layer is generally only detectable with lateral force imaging, suggesting a negligible height but a noticeable difference in frictional characteristics compared to graphite or the β-$(ET)_2I_3$ monolayer.